Role of integrin adhesions in cellular mechanotransduction

Balcıoğlu, H.E.

Chapter 5

Identification of genes regulating cellular traction forces, adhesion dynamics, and cell migration [1]

[1]This chapter is based on: Michiel Fokkelman*, Hayri E Balcıoğlu*, Janna E Klip, Kuan Yan, Fons J Verbeek, Erik HJ Danen, Bob van de Water *In Preparation; *:These authors contributed equally to this work.*

Abstract

Cell migration contributes to cancer metastasis and may also drive aspects of tumor growth. Here we aimed to identify genes controlling aspects of tumor cell migration, including the dynamic organization of cell matrix adhesions and cellular traction forces. In a siRNA screen, we identify 200+ genes that regulate size and/or dynamics of cell matrix adhesions in MCF7 breast cancer cells. In a subsequent screen, 11 of the 64 most effective genes are identified that regulate IGF1-induced 2D random cell migration of MCF7-IGF1R cells. For 4 of these hits (TPM1, PPP1R12B, HIPK3 and RAC2), whose silencing led to significantly enlarged adhesions and reduced cell migration, we studied their role in traction force generation. Silencing PPP1R12B, HIPK3 or RAC2 led to enhanced traction forces. Moreover, the force turnover was considerably reduced in adhesions following knockdown of these genes. Taken together, we identify genes that co-regulate cell migration, cell matrix adhesion dynamics and traction force turnover. Targeting PPP1R12B, HIPK3 or RAC2, results in large adhesions that are associated with high static traction forces and effectively blocks cell migration.

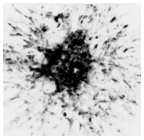

5.1 Introduction

Cell migration plays an important role in physiological processes, such as embryonic development, skin renewal and immune response. Deregulation of this cellular process plays a role in various pathologies, including cancer[1]. Tumor metastasis is the most lethal aspect of cancer progression and involves tumor cell invasion and dissemination [2]. Moreover, modeling has shown that short-range migration contributes to mixing of cell clones inside the tumor thereby promoting tumor growth [3]. Thus, oncogenic signaling pathways causing enhanced tumor cell migration *in vitro* may contain candidate targets for blocking tumor growth and metastasis formation *in vivo*. Established pathways in this respect include mitogen-activated protein kinase/extracellular signal-regulated kinase (MAPK/ERK) pathway and phosphatidylinositol 3-kinase (PI3K) [4, 5]. In addition to supporting cell survival and proliferation, these pathways also regulate cell adhesion and actin cytoskeleton [6].

Cell migration on 2D environments typically consists of several steps: protrusion, attachment, cell body movement and tail retraction [7]. Cell matrix adhesion dynamics and remodeling of the actin cytoskeleton plays a role in all of these processes [8]. Cell protrusions are driven by actin polymerization [9] and stabilized by attachment of the leading edge to the underlying surface through integrin mediated cell matrix adhesions. These adhesions contain a dynamic integrin-associated multiprotein complex that locally couples the extracellular matrix (ECM) to the actin cytoskeleton and, through cytoskeletal connections with the nuclear membrane, to the nucleus [10]. Cell body movement is driven through contractile actomyosin bundles that pull the cell body and nucleus towards the leading edge [11]. Finally the trailing edge is retracted by inducing cell matrix adhesion disassembly, possibly through microtubule signaling [12].

Formation of cell matrix adhesions and the actomyosin contractile machinery have also been shown to mediate some forms of cell migration in 3D [13]. However, the paradigm of 2D cell migration does not translate well to all 3D environments and (tumor) cells show a high level of plasticity allowing them to switch between different modes of migration in 3D [14, 15]. 3D cell confinements allow migration strategies that are independent of integrin-mediated cellular attachment [13, 16]. It has been reported that membrane protrusion formation, rather than motility in 2D corresponds to cell migration capacity in 3D [17].

Here, we aimed to understand the underlying machinery of tumor cell migration and its relation to adhesion turnover and cellular traction forces. In an siRNA screen, we identify 200+ genes that regulate size and/or dynamics of cell matrix adhesions in MCF7 breast cancer cells. In a subsequent screen, 11 of the 64 most effective genes are identified that regulate IGF1-induced 2D random cell migration of MCF7-IGF1R cells. For 4 of these hits (TPM1, PPP1R12B, HIPK3 and RAC2), whose silencing led to significantly enlarged adhesions and reduced cell migration, we studied their role in traction force generation. Silencing PPP1R12B, HIPK3 or RAC2 led to enhanced traction forces. Moreover, the force turnover was considerably reduced following knockdown of these genes. Taken together, we identify genes that co-regulate cell migration, cell matrix adhesion dynamics and traction force turnover. Targeting PPP1R12B, HIPK3 or RAC2, results in large adhesions that are associated with high static traction forces and effectively blocks cell migration.

5.2 Results

5.2.1 Larger adhesions and altered adhesion dynamics in response to knockdown of TPM1, PPP1R12B, RAC2 or HIPK3

To identify genes regulating cell matrix adhesion dynamics, a nocodazole assay was performed in MCF7 cells transfected with siRNA SMARTpools targeting adhesome genes. Four hours of nocodazole treatment resulted in disassembly of the microtubule network and after washout of nocodazole followed by incubation for 2 hours in DMSO, the microtubule network reassembled as described earlier [18] (Figure 5.1A, top). This corresponded with appearance of a more prominent actin network and larger cell matrix adhesions in the presence of nocodazole, a phenotype that was reversed after nocodazole washout (Figure 5.1A, middle and bottom). Automated quantitative analysis software was applied to identify individual adhesions and nuclei (Figure 5.1B). This confirmed growth of cell matrix adhesions in the presence of nocodazole and reversion to sizes comparable to DMSO condition upon washout (Figure 5.1C - mock). Knockdown of candidate genes with SMARTpools resulted in altered responses to nocodazole treatment and washout (Figure S1). 64 SMARTpools markedly affecting the response were further investigated.

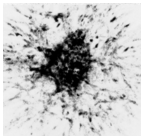

Results of four of these SMARTpools that led to enlarged cell matrix adhesions under control conditions are shown (Figure 5.1C-E). Knockdown of HIPK3, although leading to larger adhesions did not affect the response to nocodazole or washout, indicating that cell matrix adhesion dynamics were not disturbed (Figure 5.1C). Knockdown of TPM1 did not affect cell matrix adhesion growth in response to nocodazole but shrinkage after nocodazale washout was reduced, suggesting partially impaired adhesion disassembly (Figure 5.1C). PPP1R12B knockdown led to a less prominent enlargement of adhesions in response to nocodazole and after washout adhesions were much smaller than in the DMSO condition, suggesting impaired dynamic adhesion growth (Figure 5.1C). Knockdown of RAC2 completely blocked cell matrix adhesion growth in response to nocodazole, indicating a block in general cell matrix adhesion dynamics (Figure 5.1C).

5.2.2 Knockdown of TPM1, PPP1R12B, RAC2 or HIPK3 inhibits tumor cell migration

All 64 candidate genes identified with the nocodazole assay, were silenced with siRNA SMARTpools and migration of individual MCF7-IGF1R cells stimulated with IGF1 was quantified (Figure 5.2A). Positive control si-DNM2 [19] significantly reduced cell migration when compared to mock condition as expected. The knockdown of 18 candidate genes significantly impaired cell migration whereas knockdown of 5 genes enhanced cell migration (Figure 5.2A). In a deconvolution screen using 4 individual siRNAs, 11 of the hits identified in the nocodazole and random cell migration assays were confirmed, including reduced cell migration in the presence of siRNAs targeting TPM1, PPP1R12B, RAC2 or HIPK3 (Figure 5.2B,C and data not shown). Vinculin immunostaining on cells fixed after the random migration assay further confirmed that larger adhesions were formed following the knockdown of TPM1, PPP1R12B, RAC2 or HIPK3 (Figure 5.2D-F).

5.2.3 Knockdown of PPP1R12B, RAC2 and HIPK3 results in higher traction forces and slower force turnover

After establishing the importance of TPM1, PPP1R12B, RAC2 and HIPK3 in cell matrix adhesion dynamics and cell migration, we wanted

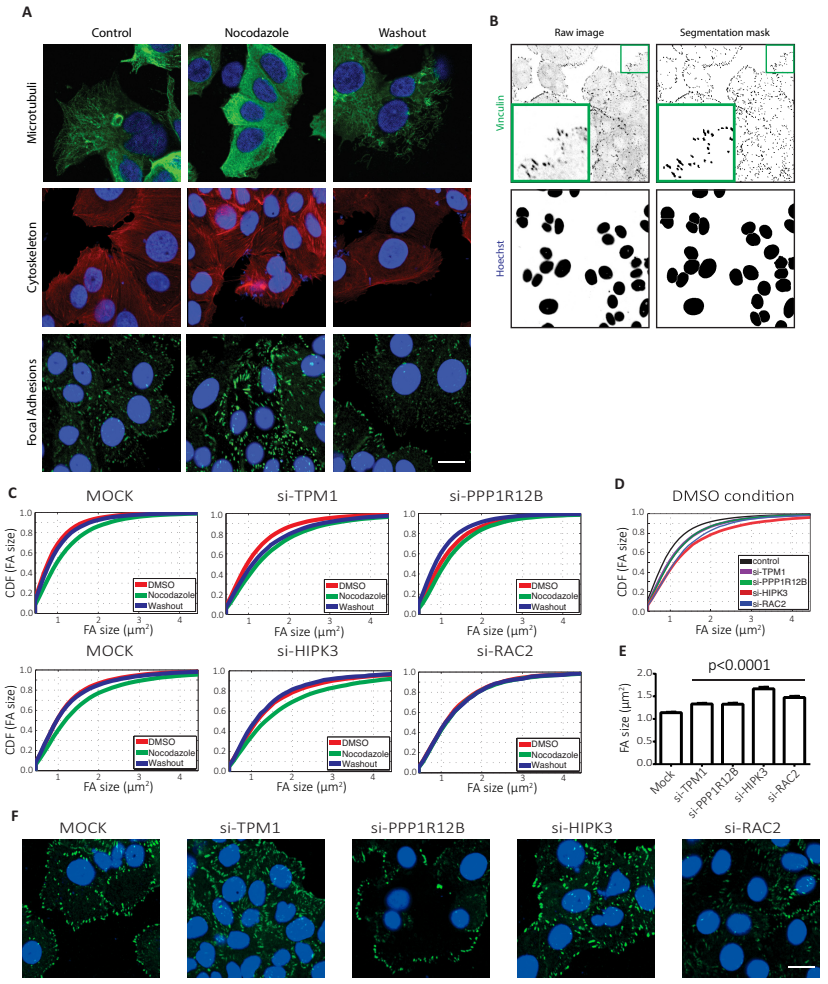

Figure 5.1

Nocodazole assay identifies genes responsible in cell-matrix adhesion dynamics. *A, MCF7 cells stained for microtubules (top), actin (middle) or vinculin (bottom) together with nucleus staining in blue in control DMSO condition (left), following 4 hours of nocodazole treatment (middle) or after washout of nocodazole and refreshment with control medium (right). B, Representative images of vinculin (top) and nucleus (bottom) on the left panel and corresponding binary images obtained following automated analysis on the right. C, Cumulative distribution functions of sizes of adhesions obtained by automated analysis shown in B, in mock condition or following siRNA knockdowns of indicated genes for the conditions mentioned in A. D-F, cumulative distribution functions of adhesion sizes in DMSO condition indicated in C (D), corresponding bar graphs showing mean and 95% confidence interval (E), and representative images showing vinculin in green and nucleus in blue (F). Scale bar is 20 µm. p value in E was calculated by comparing the knockdown conditions to the mock condition using t-test with Welch correction.*

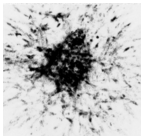

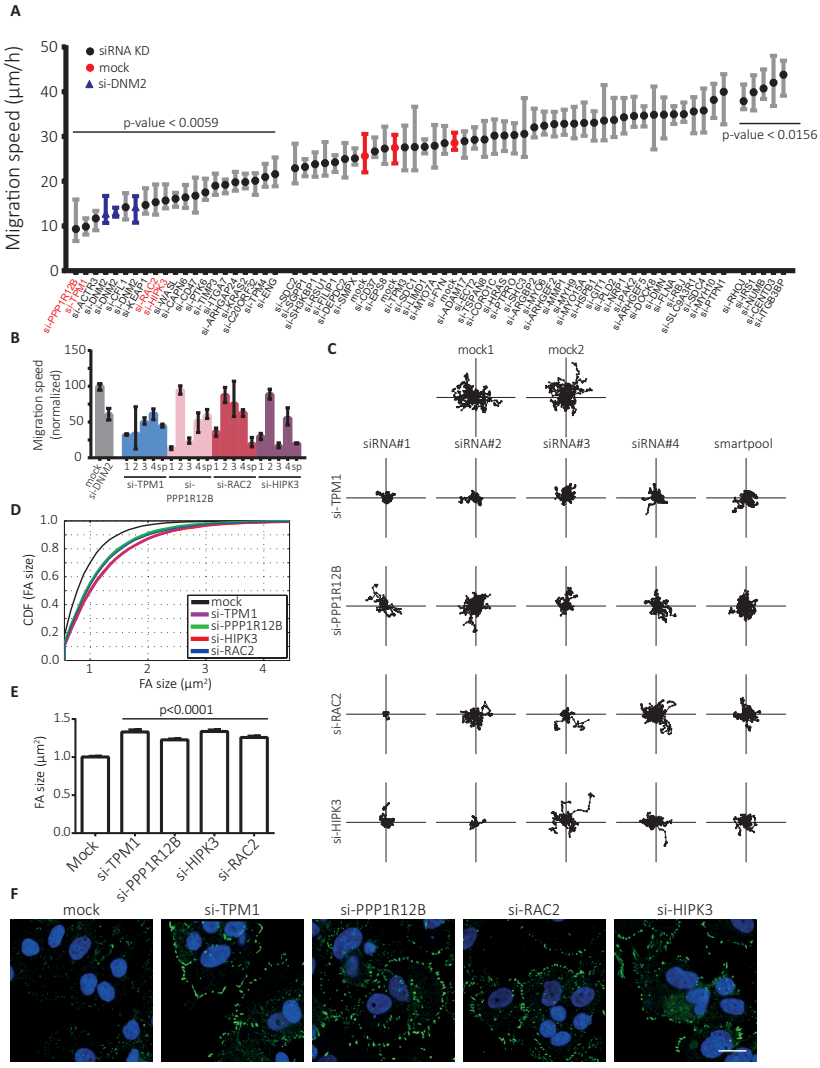

Figure 5.2

Disrupted cell matrix adhesion organization affects cell migration. *A, Quantification of single cell migration speed of MCF7-IGF1R cells after SMARTpool siRNA knockdown of 64 hits. B, C, Quantification of single cell migration speed normalized to mock following knockdown with single siRNA sequences or SMARTpool knockdown (B) and trajectories of individual cells (C). D-F, cumulative distribution functions of adhesion sizes for MCF-IGF1R cells with indicated SMARTpool knockdowns fixed after cell migration assay (D), corresponding bar graphs (E), and representative images showing vinculin in green and nucleus in blue (F). Scale bar is 20 µm. Median (A, B) or mean (E) and 95% confidence interval is shown. p values were calculated by comparing the knockdown conditions to the mock condition either with Kruskal-Wallis test with Dunn's post correction (A) or t-test with Welch correction (E).*

to study the role of these proteins in cellular force application. In order to visualize the actin cytoskeleton, MCF7-IGF1R cells were transduced with a lentiviral vector to stably express mCherry-LifeAct. Following transient transfection with siRNAs, MCF7-IGF1R-mCherry-LifeAct cells were seeded on fibronectin-stamped PDMS micropillars with an effective Young's Modulus of 47.2 kPa (bending stiffness of 65.8 nN/µm), stimulated with IGF1 and cellular forces were recorded (Figure 5.3A). The force per pillar was analyzed for the duration of the experiment (Figure 5.3B). Forces applied in PPP1R12B, RAC2 and HIPK3 knockdown conditions were significantly higher than those measured in the mock condition whereas TPM1 knockdown did not result in a significant change in magnitude of cellular traction forces (Figure 5.3C). To assess whether this reflected a general response of the entire population or whether localized increases in force were involved, we analyzed the cumulative distribution function (cdf) of measured traction forces. In addition to a shift in the population towards higher traction forces following PPP1R12B, RAC2 and HIPK3 knockdown, knockdown of each of these genes resulted in wider distributions (Figure 5.3D). This indicated that there is a larger heterogeneity in traction forces applied at different cellular regions, in response to knockdown of these genes.

Lastly, to determine the role of these genes in adhesion force turnover, we determined the autocorrelation of the force magnitudes measured at individual pillars over time. The autocorrelation function provided information on the duration of forces transduced by cellular adhesions, with faster decays indicating that the forces applied through adhesions were changing rapidly. The resulting autocorrelation functions showed the steepest decrease for the mock condition (Figure 5.3E). Quantification of the autocorrelation function halftimes showed a force halftime of ∼22 minutes for the mock condition (Figure 5.3F). The halftime was increased by ∼50% after silencing of TPM1 (although for this condition the increase was not significant), PPP1R12B or HIPK3 genes and, in addition to its most prominent attenuation of cell matrix adhesion dynamics (Figure 5.1C), knockdown of RAC2 led to doubling of the halftime up to >45 minutes (Figure 5.3F).

These findings indicate that out of 4 genes relevant for adhesion dynamics and cell migration, PPP1R12B, HIPK3 and RAC2 regulate force amplitude and turnover at cell matrix adhesions.

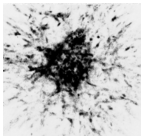

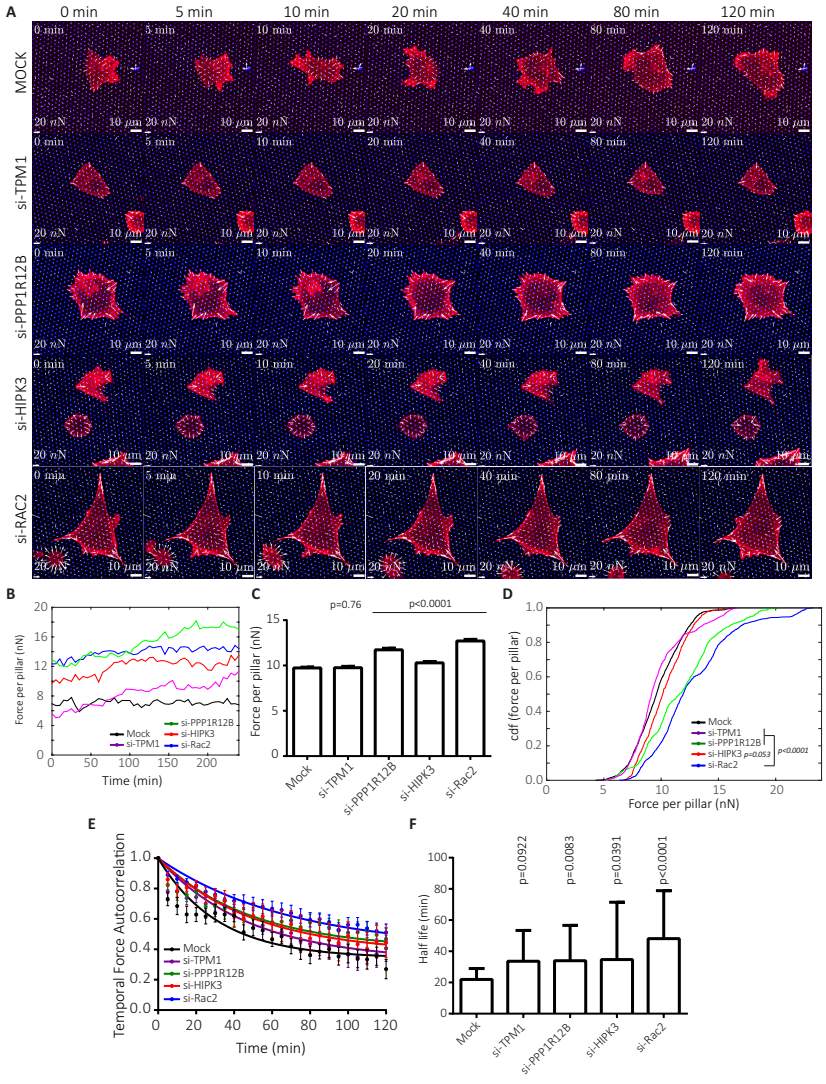

Figure 5.3

Knockdown of PPP1R12B, HIPK3 and RAC2 increases cellular force application and reduces force dynamics. *A, B, Time-lapse images of MCF7-IGF1R-mCherryLifeAct cells with indicated knockdowns together with corresponding forces at given times after IGF1 stimulation (A), and quantification of forces applied on top 5% deflected pillars followed throughout the experiment (B). C, D, bar graphs showing mean and 95% confidence interval (C), and corresponding cumulative distribution functions (D) of force per pillar for indicated SMARTpools. E, F, Force per pillar autocorrelations and corresponding fits using single exponential decay function for indicated knockdowns (E), and calculated half-times from the exponential fits with calculated errors (F). Scale bars are 20 nN and 10 µm. p values were calculated either by comparing means (C) or standard deviations (D) to mock condition using t-test with Welch's correction (C, D) or using extra sum of squares f-test (F).*

5.3 Discussion

New insights into cell adhesion and migration are a starting point for identification of drug targets implicated in cancer progression. Our findings relate the dynamics of cell matrix adhesions and the dynamics of cellular traction forces generated at these sites to tumor cell migration. We identify PPP1R12B, HIPK3 and RAC2 as regulators of each of these processes.

Even though we could not establish a role for TPM1 in traction force dynamics, the TPM1 gene was identified in our primary screen for regulators of cell matrix adhesion dynamics and TPM1 knockdown also attenuated cell migration. TPM1 gene codes for tropomyosin 1. Tropomyosin 1 takes part in muscle regulation, stabilizes actin cytoskeleton in non-muscle cells and its deregulation is implicated in cardiac illnesses [20]. Opposing findings have been reported for its function in tumor cell migration. Down-regulation of TPM1 has been shown to induce [21, 22] as well as impair cell motility. This may be related to the fact that different TPM1 isoforms have opposing effects on actin organization [23]. Therefore expression of different TPM1 isoforms in tumors of various backgrounds might act as a promoter or suppressor of cancer progression. Our findings show that down-regulation of TPM1 results in larger adhesions and impairment of cell migration. Although the siRNA SMARTpool targets multiple TPM1 species, this suggests that the main TPM1 isoform affected in MCF7 cells is the TPM1λ isoform [23]. Interestingly, despite the role of tropomyosin in actin organization and previous finding of tropomyosin inducing actomyosin contractility [20, 24], we did not find significant changes in applied forces or force dynamics upon TPM1 gene silencing.

The PPP1R12B gene, also known as MYPT2, codes for myosin phosphatase target 2 (MYPT2), which takes part in the myosin phosphatase protein complex. The myosin phosphatase protein complex, together with myosin light chain kinase, orchestrates myosin regulatory light chain phosphorylation. In heart muscle, this controls normal cardiac performance [25] and is involved in the sarcomeric architecture of actin cytoskeleton [26, 27]. Given the inhibitory effect of myosin phosphatase on myosin activity, one would expect the down-regulation of PPP1R12B to induce higher traction force generation. Indeed, we show that knockdown of PPP1R12B results in higher forces as expected. In addition, it leads to formation of larger cell-matrix adhesions and significantly im-

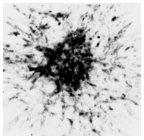

pairs force turnover. We further demonstrate that down regulation of PPP1R12B impairs tumor cell migration, possibly through its influence on cellular force machinery and adhesion dynamics.

HIPK3 encodes for the protein homeodomain interacting protein kinase 3. HIPK3 is involved in cell survival and insulin metabolism [28, 29]. Higher HIPK3 expression correlates with worse prognosis and lower sensitivity to chemotherapy [30, 31]. Here we show that knockdown of this gene also impairs tumor cell migration, induces formation of larger adhesions as well as inducing cellular force application and stability. Others have previously reported targeting HIPK3 induces sensitisization to chemotherapy[31], our findings further indicate HIPK3 as a possible target to impair tumor metastasis.

RAC2 encodes Ras-related C3 botulinum toxin substrate 2 (Rac2), and is a member of Rho family of GTPases that regulate actin cytoskeleton [32]. Rac2 knockout in the tumor stroma is known to regulate tumor growth and metastasis [33] and activating mutations have been identified in human cancer [34]. Previously, Rac2 knockout macrophages were shown to display altered migration and fewer podosomal structures, indicative of increased contractility [35, 36]. Our findings extend these studies: Rac2 is implicated in cancer cell migration and in its absence cell matrix adhesions become static and cellular traction forces at these sites are increased and very stable.

A positive correlation between adhesion size and the magnitude of cellular forces has been reported previously [37–39]. Our results confirm this notion and identify 3 important regulators of these aspects. Interestingly, these regulators also control the dynamics of traction forces: their downregulation leads to decreased force turnover rates. Small dynamic cell matrix adhesions and low dynamic traction forces go hand in hand with an active actin cytoskeleton organization that drives cellular motility. Genes, such as the ones identified here, that regulate these aspects and whose silencing causes a shift to larger adhesions with high stable traction forces causing inhibition of cell migration; encode candidate targets to interfere with tumor metastasis. Since cell motility in 3D environments is highly plastic and may follow a different set of rules [13, 14], it remains to be established what the consequences of their inhibition are under such conditions. Such studies followed by preclinical animal models will have to further establish their potential as cancer drug targets.

5.4 Materials and methods

5.4.1 Cell culture

MCF7 and IGF1R overexpressing MCF7-IGF1R cell lines described previously [40], were grown in RPMI1640 medium supplemented with 10% fetal bovine serum (GIBCO, USA), 25 U/ml penicillin and 25 µg/ml streptomycin (Invitrogen) in a 5% CO2 humidified incubator at 37°C. For visualization of the actin cytoskeleton, cells were transduced using a lentiviral mCherry-LifeAct cDNA expression vector (provided by Dr. Olivier Pertz, University of Basel, Basel, Switzerland), and were cultured in selection medium containing 2 µg/ml puromycin (Acros Organics/Fisher Scientific cat. # 227420500).

5.4.2 Cell transfection with siRNA

A custom designed SMARTpool siRNA library (Dharmacon, Lafayette, CO, USA) targeting 569 genes with known or predicted roles in cell adhesion was used. The siRNAs were diluted with serum free medium (SFM) together with DharmaFECT 4 (Dharmacon). Glass bottom 96-well plates (Greiner Bio-One, Frickenhausen, Germany) were coated with 10 µg/ml Collagen type 1 (isolated from rat tails). A 50 nM reverse transfection was performed according to manufacturer's guidelines. Complex formation time was 20 minutes and 10,000 MCF7 WT cells were added. Transfection was performed in duplicate. Each plate contained negative controls (no siRNA, mock, siGFP (D-001300-01) and non-targeting Control #2 (D-001210-02)), a positive control (si-DNM2) and transfection controls (si-KIF11, si-PXN and si-GLO Green). Plates were placed in the incubator and the medium was refreshed after 20 hours.

Cells were put on overnight serum starvation 32 hours after transfection. The next day, a nocodazole assay was performed, in which cells were exposed to one of three conditions. Cells were exposed either to 0.025% DMSO in starvation medium for 6 hours, or to 10 µM nocodazole (#74151, Fluka, Sigma-Aldrich, St.Louis, MO, USA) in starvation medium for 4 hours, or to 4 hours 10 µM nocodazole followed by a 2 hours washout with 0.025% DMSO in starvation medium. Transfection controls (si-KIF11, si-PXN and si-GLO Green) were not exposed. After treatment, cells were fixed in 4% buffered formaldehyde for 10 minutes, and washed thrice with PBS. Fixed cells were permeabilized

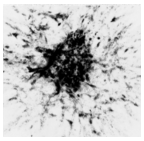

and blocked in TBP (0.1% Triton X-100, 0.5% BSA in PBS), followed by immunostaining for vinculin (V-9131, Sigma-Aldrich), tubulin (T-9026, Sigma-Aldrich) or Rhodamine Phalloidin (Invitrogen/Fisher Scientific cat. number R415), and by secondary antibody conjugated with Alexa488 (Invitrogen/Fisher Scientific cat. number A11008). Hoechst 33258 (Sigma) was used to visualize nuclei.

5.4.3 Automated microscopy

Microscopy was performed on a Nikon Eclipse Ti confocal microscope that included an automated xy-stage, an integrated Perfect Focus System (PFS) and 408, 488 and 561 Argon lasers. The system was controlled by Nikon's EZ-C1 software (version 3.90). Images were acquired using a Plan-Apochromat 20x objective with 0.75 NA, at a resolution of 512 x 512 pixels, with a pixel dwell time of 7 µs and 4x scanner zoom.

For automated imaging, a custom-written macro was used within EZ-C1 that searched for cells, focus on the focal adhesions and acquire an image. Using the Perfect Focus System, the software searches randomly for cells in Hoechst channel (408-laser) until a certain threshold is met, i.e. a number of cells per well (pre-set). The PFS is then turned off, and using a custom autofocus it focuses on the focal adhesions. Once the optimal focus is found, the system acquires the image and then continues with the next position. Between 5 and 8 images per well were acquired.

5.4.4 Image analysis

Image analysis was implemented using ImageJ version 1.43h (http://imagej.nih.gov/ij/). Acquired images were split into the original channels and the nuclei channel was used to remove empty images. The analysis was performed for one channel at a time. First, the image is passed through a Gaussian filter to normalize the CCD signal and a rolling ball is applied to remove noise. Next, segmentation was performed based on a watershed masked clustering algorithm [41]. Cell matrix adhesion features: area, perimeter, extension, dispersion, elongation, orientation, compact factor and average intensity, were obtained for objects larger than 4 pixels.

5.4.5 Random cell migration assay

MCF7-IGF1R cells were used for live cell migration assays. Transfections were performed as described above, with 15,000 cells in a standard 96-well culture plate. After 56 hours, the transfected MCF7-IGF1R cells were replated onto collagen-coated glass bottom plates and were allowed to adhere overnight. Cells were switched to starvation medium and pre-exposed for 45 minutes to 100 ng/ml Hoechst 33342. After refreshing the medium, cells were placed on a Nikon Eclipse Ti microscope fitted with a 37°C incubation chamber, 20x objective (0.75 NA), automated stage and PFS system.

Three positions per well were manually selected, and Differential Interference Contract (DIC) and Hoechst images were captured every 6 to 14 minutes with a DS-Qi1MC CCD camera with 2x2 binning (pixel size: 0.64 µm) for 7 hours using NIS software (Nikon) following stimulation with 100 ng/ml IGF1 (Increlex, Ipsen, Basking Ridge, NJ, USA). All images were sorted using custom-made R-scripts (R Foundation for Statistical Computing, Vienna, Austria). Image analysis was performed using CellProfiler (Broad Institute [42]). Briefly, images were segmented using a watershed masked clustering algorithm, after which cells were tracked based on overlap between frames. Tracking data was organized and analyzed using in-house developed R-scripts [43] to obtain single cell migration data. Single cell migration speeds were plotted using GraphPad Prism 6.0 (GraphPad Software, La Jolla, CA, USA) and changes in migration speed were evaluated by comparing cell populations (Kruskal-Wallis with Dunn's multiple comparisons post-test). For all live microscopy, experiments were performed in duplicate and results were considered significant if p-value < 0.05 for all experiments.

Visualization and analysis of cell matrix adhesions was performed as described for nocodazole assay.

5.4.6 Traction force microscopy with silicon elastomeric micropillar post arrays

MCF7-IGF1R-mCherry-LifeAct cells were transfected with siRNAs as described above. After 65h, cells were used for micropillar experiments, according to methodology described previously [44]. Nanolithography with PDMS was performed to create pillars of 4.1 µm height, 2 µm diameter, 4 µm center-to-center distance in a hexagonal lattice with spac-

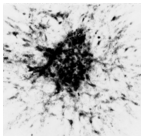

ers on the side. Pillars were calculated to have a bending stiffness of 65.8 nN/µm and an effective Young's modulus of 47.2 kPa [44]. ECM stamping was performed using a flat piece of PDMS preincubated with a 40 µl mix of [50 µg/mL unlabeled fibronectin (Sigma Aldrich) and 10 µg/mL Alexa647 (Invitrogen)-conjugated fibronectin]. Following blocking with 0.2% Pluronic (F-127, Sigma Aldrich) in PBS for 1 hour, cells were pipetted on the pillar array and were incubated for 2 hours in complete medium, and 3 hours in serum starved medium. For imaging, the pillars, with cells on top, were placed upside down in a 24 well glass bottom plate (Greiner Bio-One), mounted on a Nikon Eclipse Ti microscope, stimulated with 100 ng/mL IGF1 and imaged every 5 minutes for 400 minutes in scanning confocal mode together with a 20x magnification 0.75 NA dry air lens with internal 1.5 x magnification and 4.184 scanner zoom to obtain a pixel size of 0.2 µm.

Forces were calculated with approximately 2 nN precision from the pillar channel using specifically designed Matlab scripts (Mathworks, Natick, MA, USA) as described previously [44]. Briefly, deflections of individual pillars were calculated by relating the exact pillar locations determined from the labeled fibronectin fluorescence image to the calculated reference undeflected hexagonal grid. Movies were generated and manually checked for movies with deflections that had high signal-to-noise ratio and to remove cells that died or divided. Cell masks were generated from the mCherry-LifeAct channel by first passing the image through a Gaussian low pass filter, subtracting the background intensity and running the image through a sobel and a log-edge detection algorithm followed by image dilation and hole filling each time. Pillars were followed through the movie with in-house written Matlab script that matched pillars in subsequent frames (or 2 frames apart if a match was not found in first iteration) that were closer than 2 µm. This enabled tracking more than 90% of the pillars for the duration of the movie. Pillars that showed the top 5% deflection for the duration of the imaging and were coupled to cells were taken for further analysis. Average force per pillar was determined by averaging the pillar deflections for the whole duration of the movie for all selected cells. Autocorrelation was calculated for top 5% deflected pillars per movie using Matlab acorr function, averaged per condition and an exponential function was fit for the first 2 hours (25 data points) to obtain the half time.

5.4.7 Statistic analysis

Significance was calculated according to the method indicated at individual figure legends using GraphPad Prism 6.0.

5.5 Acknowledgements

We thank Olivier Pertz for providing the mCherry-LifeAct construct; Kees van Oord for developing an automated FA imaging macro for EZ-C1; Hans de Bont for technical assistance with live microscopy; Sandra Zovko for help with IF staining and study design; and Sylvia Le Dévédec for her helpful comments on the manuscript. This work was financially supported by grants from the EU FP7 Health Programs MetaFight project (grant agreement 201862) to B. van de Water; Systems Microscopy NoE project (grant agreement 258068) to B. van de Water; and the Netherlands Organization for Scientific Research NWO-FOM (grant number 09MMC03 to H.E.B.).

5.6 Authors' contribution

MF, HEB, EHJD and BvdW designed the research and wrote the manuscript. MF, HEB and JEK performed the experiments and analyses. KY and FJV established the FA image analysis tools.

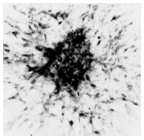

5.7 Supplemental figures

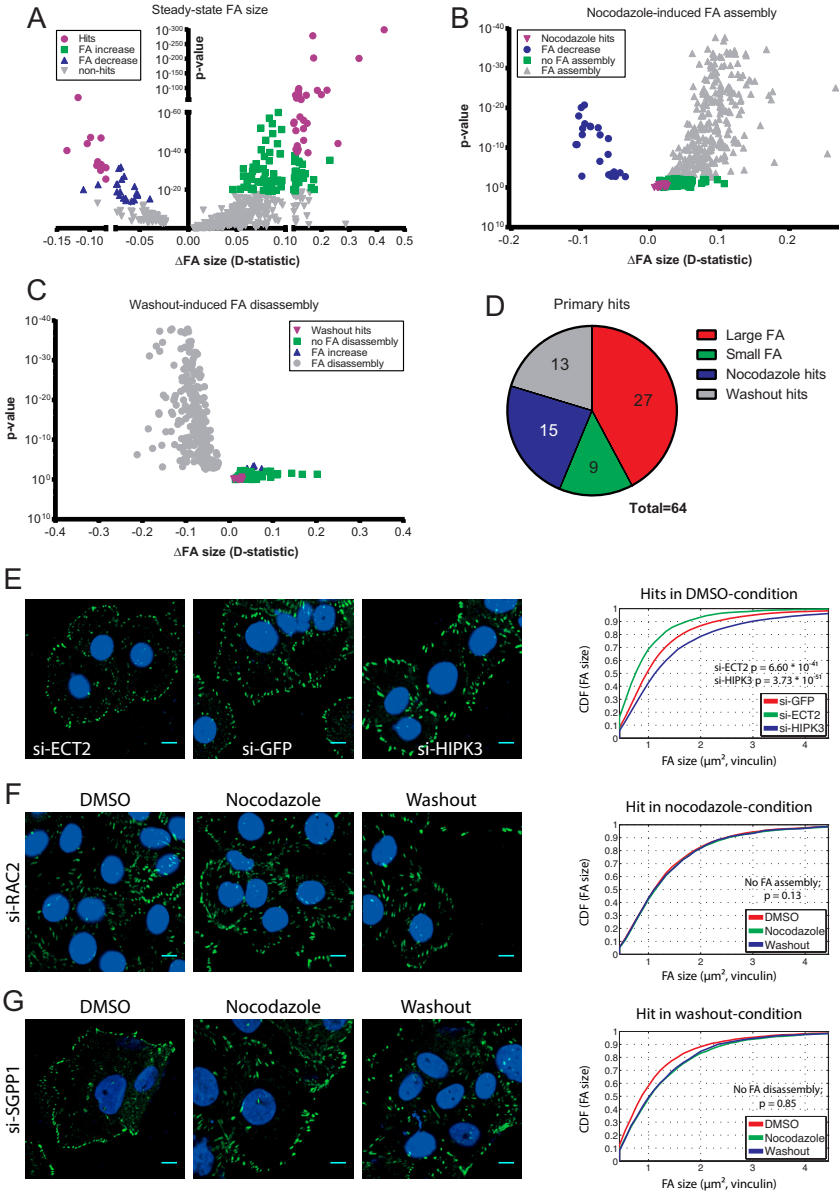

Figure S1
RNAi screen identifies novel regulators of cell matrix adhesion dynamics.

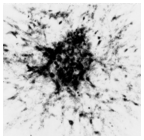

Figure S1

RNAi screen identifies novel regulators of cell matrix adhesion dynamics. *A, Cell matrix adhesion size distributions after siRNA knockdown in DMSO condition were compared to siGFP control cells. The shift in size distribution (D-statistic) is used as a measurement of change in adhesion size. A decrease in adhesion size is shown in blue and an increase in size in green. Hits remaining after stringent thresholding are shown in purple. B, Cell matrix adhesion size of siRNA knockdown cells in nocodazole condition was compared to DMSO of the same siRNA, to detect impaired adhesion assembly. siRNAs that show no change in FA size were considered as hits (purple). C, Cell matrix adhesion size of siRNA knockdown cells in washout condition was compared to nocodazole of the same siRNA, to detect impaired adhesion disassembly. siRNAs that show no change in adhesion size were considered as hits (purple). D, In total 64 hits were found to affect cell matrix adhesion morphology under steady state conditions (red and green), or to specifically impair adhesion assembly (blue) or disassembly (grey). E, Example images of adhesion size decrease (si-ECT2) and increase (si-HIPK3) after siRNA knockdown in DMSO condition. Quantification of adhesion size is shown on the right. F, Loss of RAC2 inhibited cell matrix adhesion assembly. Quantification of adhesion size shows identical distributions in the different conditions. G, Knockdown of SGPP1 impaired adhesion disassembly. Quantification of adhesion sizes confirms no change in washout condition compared to nocodazole.*

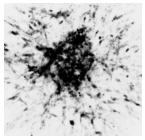

Bibliography

[1] Anne J Ridley et al. "Cell migration: Integrating signals from front to back". In: *Science (New York, N.Y.)* 302.5651 (2003).

[2] Daniela Quail and Johanna Joyce. "Microenvironmental regulation of tumor progression and metastasis". In: *Nature Medicine* 19.11 (2013).

[3] Bartlomiej Waclaw et al. "A spatial model predicts that dispersal and cell turnover limit intratumour heterogeneity". In: *Nature* 525.7568 (2015).

[4] Amardeep S Dhillon et al. "MAP kinase signalling pathways in cancer". In: *Oncogene* 26.22 (2007).

[5] Ana M Gonzalez-Angulo et al. "PI3K pathway mutations and PTEN levels in primary and metastatic breast cancer". In: *Molecular Cancer Therapeutics* 10.6 (2011).

[6] Cai Huang, Ken Jacobson, and Michael D Schaller. "MAP kinases and cell migration". In: *Journal of Cell Science* 117.20 (2004).

[7] J Thomas Parsons, Alan R Horwitz, and Martin A Schwartz. "Cell adhesion: integrating cytoskeletal dynamics and cellular tension." In: *Nature Reviews. Molecular Cell Biology* 11.9 (2010).

[8] Christophe Clainche and Marie-France Carlier. "Regulation of actin assembly associated with protrusion and adhesion in cell migration". In: *Physiological Reviews* 88.2 (2008).

[9] Corina Sarmiento et al. "WASP family members and formin proteins coordinate regulation of cell protrusions in carcinoma cells". In: *The Journal of Cell Biology* 180.6 (2008).

[10] Benjamin Geiger, Joachim Spatz, and Alexander Bershadsky. "Environmental sensing through focal adhesions". In: *Nature Reviews Molecular Cell Biology* 10.1 (2009).

[11] Hideki Yamaguchi and John Condeelis. "Regulation of the actin cytoskeleton in cancer cell migration and invasion". In: *Biochimica et Biophysica Acta (BBA) - Molecular Cell Research* 1773.5 (2006).

[12] Sandrine Etienne-Manneville. "Microtubules in cell migration". In: *Cell and Developmental Biology* 29.1 (2012).

[13] Ryan J Petrie et al. "Nonpolarized signaling reveals two distinct modes of 3D cell migration". In: *The Journal of Cell Biology* 197.3 (2012).

[14] Peter Friedl et al. "New dimensions in cell migration." In: *Nature Reviews. Molecular Cell Biology* 13.11 (2012).

[15] Hoa H Truong et al. "β1 integrin inhibition elicits a prometastatic switch through the TGFβ-miR-200-ZEB network in E-cadherin-positive triple-negative breast cancer". In: *Science Signaling* 7.312 (2014).

[16] Martin Bergert et al. "Force transmission during adhesion-independent migration." In: *Nature Cell Biology* 17.4 (2015).

[17] Aaron S Meyer et al. "2D protrusion but not motility predicts growth factor–induced cancer cell migration in 3D collagen". In: *The Journal of Cell Biology* 197.6 (2012).

[18] Ellen J Ezratty, Michael A Partridge, and Gregg G Gundersen. "Microtubule-induced focal adhesion disassembly is mediated by dynamin and focal adhesion kinase." In: *Nature Cell Biology* 7.6 (2005).

[19] Wei-Ting Chao and Jeannette Kunz. "Focal adhesion disassembly requires clathrin-dependent endocytosis of integrins". In: *FEBS Letters* 583.8 (2009).

[20] Peter Gunning, Geraldine O'neill, and Edna Hardeman. "Tropomyosin-based regulation of the actin cytoskeleton in time and space". In: *Physiological Reviews* 88.1 (2008).

[21] Hua-Qing Q Du et al. "Silencing of the TPM1 gene induces radioresistance of glioma U251 cells." In: *Oncology Reports* 33.6 (2015).

[22] Qiao Zheng, Alfiya Safina, and Andrei V Bakin. "Role of high-molecular weight tropomyosins in TGF-β-mediated control of cell motility". In: *International Journal of Cancer* 122.1 (2008).

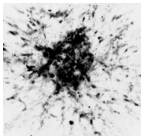

[23] Syamalima Dube et al. “Expression of tropomyosin 1 gene isoforms in human breast cancer cell lines”. In: *International Journal of Breast Cancer* 2015 (2015).

[24] Hideaki Fujita et al. “The effect of tropomyosin on force and elementary steps of the cross-bridge cycle in reconstituted bovine myocardium”. In: *The Journal of Physiology* 556.2 (2004).

[25] Audrey Chang et al. “Constitutive phosphorylation of cardiac myosin regulatory light chain in vivo”. In: *Journal of Biological Chemistry* 290.17 (2015).

[26] Takuro Arimura et al. “Identification, characterization, and functional analysis of heart-specific myosin light chain phosphatase small subunit”. In: *Journal of Biological Chemistry* 276.9 (2001).

[27] Ryuji Okamoto et al. “Characterization and function of MYPT2, a target subunit of myosin phosphatase in heart.” In: *Cellular Signalling* 18.9 (2006).

[28] Véronique Rochat-Steiner et al. “FIST/HIPK3: a Fas/FADD- interacting serine/threonine kinase that induces FADD phosphorylation and inhibits fas-mediated Jun NH(2)-terminal kinase activation.” In: *The Journal of Experimental Medicine* 192.8 (2000).

[29] Nobuhiro Shojima et al. “Depletion of homeodomain-interacting protein kinase 3 impairs insulin secretion and glucose tolerance in mice”. In: *Diabetologia* 55.12 (2012).

[30] James F Curtin and Thomas G Cotter. “JNK Regulates HIPK3 expression and promotes resistance to Fas-mediated apoptosis in DU 145 prostate carcinoma cells”. In: *Journal of Biological Chemistry* 279.17 (2004).

[31] Meng Xu et al. “miR-382 inhibits tumor growth and enhance chemosensitivity in osteosarcoma.” In: *Oncotarget* 5.19 (2014).

[32] Anne J Ridley. “Rho GTPases and actin dynamics in membrane protrusions and vesicle trafficking”. In: *Trends in Cell Biology* 16.10 (2006).

[33] Shweta Joshi et al. “Rac2 controls tumor growth, metastasis and M1-M2 macrophage differentiation in vivo.” In: *PLoS One* 9.4 (2014).

[34] Masahito Kawazu et al. “Transforming mutations of RAC guanosine triphosphatases in human cancers.” In: *Proceedings of the National Academy of Sciences of the United States of America* 110.8 (2013).

[35] Ann P Wheeler et al. “Rac1 and Rac2 regulate macrophage morphology but are not essential for migration”. In: *Journal of Cell Science* 119.13 (2006).

[36] Cheng-han Yu et al. “Integrin-matrix clusters form podosome-like adhesions in the absence of traction forces”. In: *Cell Reports* 5.5 (2013).

[37] Nathalie Q Balaban et al. “Force and focal adhesion assembly: a close relationship studied using elastic micropatterned substrates”. In: *Nature Cell Biology* 3.5 (2001).

[38] Hedde van Hoorn et al. “The nanoscale architecture of force-bearing focal adhesions”. In: *Nano Letters* 14.8 (2014).

[39] Léa Trichet et al. “Evidence of a large-scale mechanosensing mechanism for cellular adaptation to substrate stiffness”. In: *Proceedings of the National Academy of Sciences of the United States of America* 109.18 (2012).

[40] Yinghui Zhang et al. “Elevated insulin-like growth factor 1 receptor signaling induces antiestrogen resistance through the MAPK/ERK and PI3K/Akt signaling routes”. In: *Breast Cancer Research* 13.3 (2011).

[41] Zi Di et al. “Automated analysis of NF-KB nuclear translocation kinetics in high-throughput screening”. In: *PLoS One* 7.12 (2012).

[42] Anne E Carpenter et al. “CellProfiler: image analysis software for identifying and quantifying cell phenotypes”. In: *Genome Biology* 7.10 (2006).

[43] Steven Wink et al. “Quantitative high content imaging of cellular adaptive stress response pathways in toxicity for chemical safety assessment”. In: *Chemical Research in Toxicology* 27.3 (2014).

[44] Hayri E Balcıoğlu et al. “The integrin expression profile modulates orientation and dynamics of force transmission at cell-matrix adhesions.” In: *Journal of Cell Science* 128.7 (2015).